JOURNAL OF MATERIALS SCIENCE 16 (1981) 2103–2108

# Dependence of dendritic morphology on crystal structure in partially crystallized amorphous Ni–P thin films

E. VAFAEI-MAKHSOOS*
*Department of Metallurgy, Technical-Scientific University, P.O. Box 41/3752, Tehran, Iran*

Electron-beam heating was used to crystallize amorphous electrodeposited thin films of nickel phosphides with a nominal composition of 20 and 22 at % P. High-resolution dark-field microscopy showed that the morphology of the transformed films depends on the rates of electron-beam heating, temperature gradients and variations in the composition of the as-deposited sample. Two distinct types of dendritic morphologies were observed; a low-angle branching dendritic morphology with b c t $Ni_{12}P_5$ structure and a high-angle branching dendritic morphology with an unknown complex $Ni_{x_1}P_{y_1}$ structure. The low-angle branching dendritic morphology is interesting in that the transformation from the as-deposited amorphous Ni–P to the equilibrium $Ni_{12}P_5$ occurred in one step without going through any intermediary more metastable states, therefore violating the Ostwald rule. The high-angle branching morphology is interesting in that for one branch of dendrite two distinct types of crystals were observed: uniform and twin platelet (heavily striated) crystals. The crystals are layered or overlapped, indicating a two-phase layered structure.

## 1. Introduction

Crystallizing an amorphous solid is a complex process which requires more basic studies; DSC, X-ray, electrical resistivity and transmission electron microscopy (TEM) have been primarily tools for studying the transformation process [1–8]. Generally, the amorphous solid progresses through a series of metastable crystal structures until the final equilibrium crystalline state is reached. This transformation process can be categorized into two stages: in the first stage thermal energy causes short-range atomic movements and incipient crystallization of metastable crystalline structures; in the second stage thermal energy causes longer range atomic movements and decomposition to the equilibrium phases [2, 3].

It has been noted that crystallizing amorphous solids is a unique way of generating a very large number of up to now undiscovered metastable crystalline compounds. Most research workers investigating this area have proceeded by isothermally annealing films for fixed times and then performing diagnostics studies; we have adopted an alternative technique of *in situ* heating† within an electron microscope, stopping the process when a particularly interesting microstructure or crystallization was observed. This phase of study resulted in the formation of several newly discovered metastable and stable nickel phosphides with new morphologies and structures [9, 10]. The formation of various morphologies and structures must depend on a number of factors, including rates of electron-beam heating, temperature gradients and homogeneity of the as-deposited sample [9, 10].

In a previous study [9] it was observed that electrodeposited thin films of Ni–P with a nominal composition of 20 and 22 at % P were amorphous

*Present address: Iran Telecommunications Research Centre, Tehran, Iran.
†A hot stage for TEM was not available.

0022–2461/81/082103–06$02.60/0 © *1981 Chapman and Hall Ltd.* 

in the as-deposited form. Upon electron-beam heating, the films crystallized into a new metastable $Ni_xP_y$(Ni) phase (presumably "$Ni_5P_2$" [10]) with various morphologies which were independent of crystal structure. In contrast, here, a different phenomenon is reported: dependence of dendritic morphology on crystal structure.

Dendritic formation in a solidifying liquid is fairly well understood; but in the case of an amorphous solid the process is complicated by a stress state which can exist across the amorphous–crystalline interface. Willens [11] in a study on the dendritic crystallization in a non-metallic amorphous Te–15 at % Ge alloy argues that the dendritic morphology is the result of the poor thermal conductivity of the tellurium-base alloy giving rise to temperature gradients (from the heat of crystallization) during growth. In contrast, Bagley and Turnbull [12] argue that the dendritic growth in a metallic amorphous Ni–24.92 at % P alloy is the result of high electrical conductivity and therefore good thermal conductivity of the Ni–P alloy. In this paper we also report on the important parameters giving rise to formation of dendritic structures in order to contrast our results with those stated above.

## 2. Experimental details

The same procedure for preparing suitable CTEM samples of amorphous Ni–P with a nominal composition of 20 and 22 at % P was followed as was previously described [9]. Most of the *in situ* electron beam heating was done with a RCA-4A electron microscope; this older instrument is capable of directing a rather intense electron beam at the sample. Both the localized and delocalized beam heating [10] were used to produce the dendrites. After the as-deposited amorphous film was partially transformed, it was viewed in a JEOLCO 100CX scanning transmission electron microscope. For most of the study CTEM was used.

## 3. Results and discussion

In partially crystallized films with a nominal composition of 20 and 22 at % P, two types of dendritic structures were observed. The first, caused by localized beam heating of the sample, was a small-angle branching dendritic structure which forms at the interface of a crystallized zone and the amorphous region (see Fig. 1). From the selected-area diffraction pattern (see Fig. 2) of this structure the phase was identified as b c t $Ni_{12}P_5$ [10]. In this process the electron beam was focused in the centre of crystallized region during the heating stage. As the heating progressed, the crystallized zone grew radially from the beam centre; this produced spherulites centred around the electron beam. The dendritic-type morphology remained in the crystallized zone after the initial "amorphous–crystalline" front advanced to other regions. The dendritic-like crystals in the zone are several micrometres long; their long axis extends from the approximate beam centre to the "amorphous–crystalline" interface. Individual dendrite arms makes an angle of about 30° with the long radial-like axis. The arms are usually less than a micrometre long.

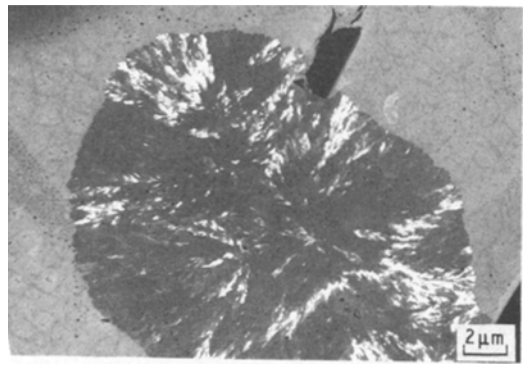


*Figure 1* Dark-field image, using the (3 3 0) reflection of Fig. 2. The crystallized zone grows dendritically, with a low-angle branching morphology, outward from the beam centre into the (grey) amorphous region.

The second type of dendritic morphology was a high-angle branching structure which was observed to be much more complicated. A selected-area diffraction pattern of the entire dendrite revealed

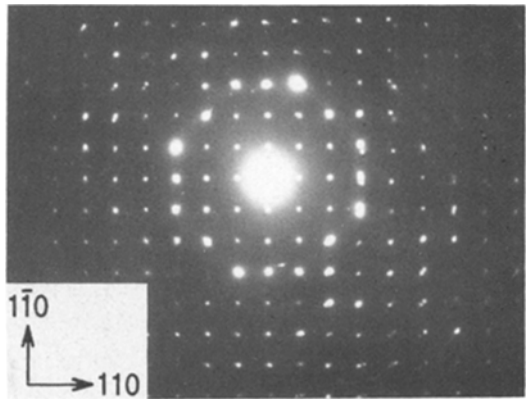


*Figure 2* The (0 0 1) projection of the reciprocal lattice of the b c t $Ni_{12}P_5$ phase.

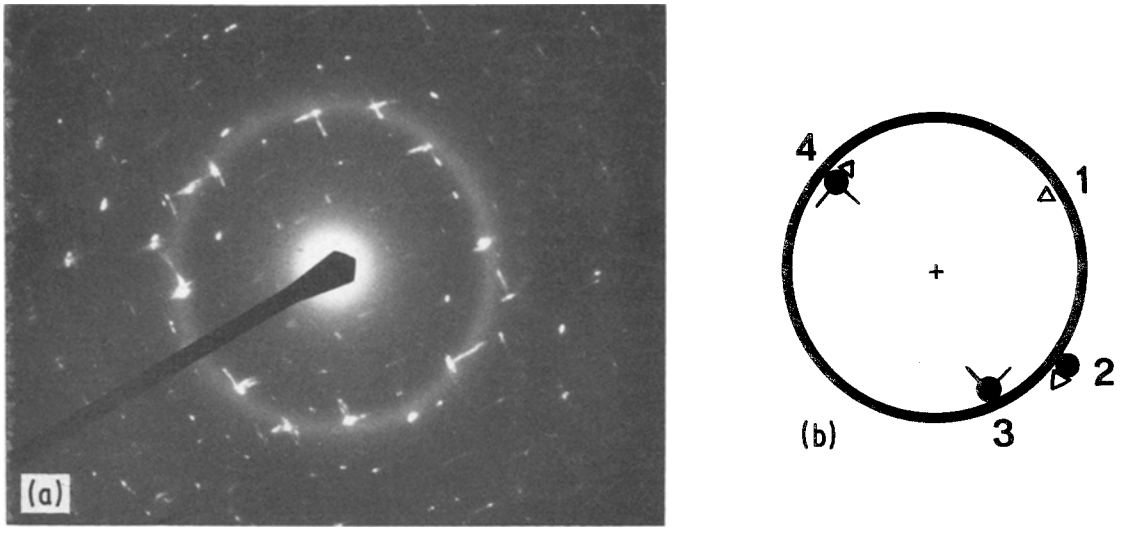


*Figure 3* (a) The electron diffraction pattern of a heavily faulted high-angle branching dendrite. Note the presence of twins and double reflections. (b) A schematic projection of part of (a). The solid curve represents the amorphous ring. Spot 1 represents a single reflection. Spot 2 represents a double reflection (a single and a matrix spot). Spot 3 represents a matrix and its twin spots. Spot 4 represents a matrix and its twin spots plus reflection due to double reflection.

a complex structure (see Fig. 3). From the selected-area diffraction pattern it was not possible to identify the phase forming the dendrite. Fig. 4 shows an overall view of a high-angle branching dendrite formed by slowly heating a large area of the film using a defocused beam (delocalized heating). The dendritic branches are heavily faulted and have a pronounced wavy texture. There are several distinct regions in which the striated lines are slightly misaligned from each other. The spacing between the lines varies from 0.6 to 1.5 nm from region to region. A second type of crystal with uniform morphology can be seen in region marked A on Fig. 4. An amorphous region marked B is enclosed by this uniform crystal and several dendritic arms. The presence of this uniform crystal in the vicinity of the dendrites is due to local variation in composition of the as-deposited films. The presence of the non-crystallized amorphous regions marked B, C and D and their resistance to crystallization are most likely due to a lower concentration ratio of Ni to P in these regions than in the crystallized regions, prior to crystallization. In other words, a high concentration of Ni will result in good conductivity of the latent heat of fusion through the amorphous matrix and the consequent lowering of temperature at the crystalline–amorphous interface. This, in turn, will enhance the process of dendrite formation.

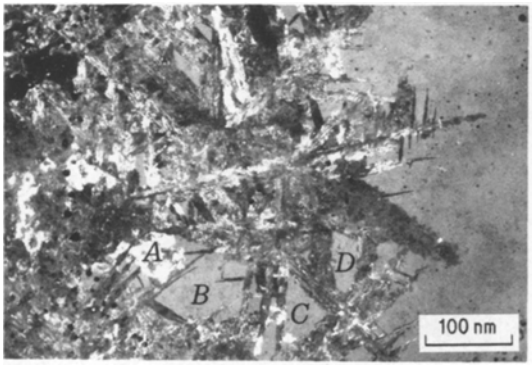


*Figure 4* The overall view of a high-angle branching dendrite formed by delocalized heating. Observe the presence of fault lines in the dendritic arms.

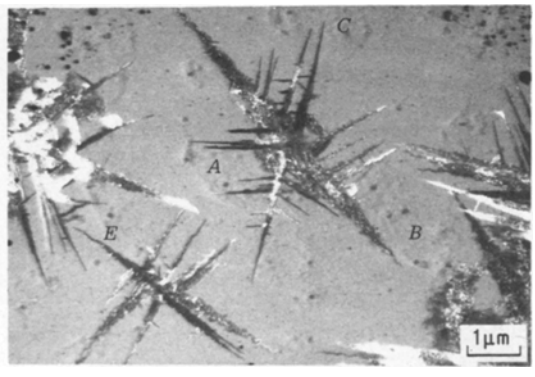


*Figure 5* The dark-field morphology of dendrites, isolated in the amorphous matrix, using reflection (4) of Fig. 3.

Fig. 5 shows another high-angle branching morphology of isolated dendrites within the amorphous matrix. This structure was formed in the vicinity of the crystallized region of Fig. 4 during heating. The presence of microcrystalline regions A, B and C within the amorphous matrix, as described previously [9], is due to inhomogeneity of the as-deposited sample. However, the individual dendrites in Fig. 5 are several micrometres long and the arms of the dendrites are now at about 60° to the main axis in some cases and 90° in others. Again, one possible explanation for the formation of these isolated dendrites within the amorphous matrix could be that it is due to the high thermal conductivity of the region where the dendritic growth initiates as compared to surrounding regions. In other words, it is believed that the dendritic growth is favoured in regions where the concentration ratio of Ni to P atoms is the highest. In fact this agrees with Bagley and Turnbull's [12] argument that the dendritic growth in a metallic amorphous Ni–24.92 at % P alloy is the result of high electrical conductivity and therefore good thermal conductivity of the Ni–P alloy. As before, the presence of the microcrystalline region marked E in the vicinity of the isolated dendrites in Fig. 5 is due to variation of composition in the as-deposited film (see Fig. 6 of [9]).

While Fig. 6, using the single reflection (1) of the diffraction pattern (Fig. 3), represents a dark-field image of rather uniform dendritic arms, Fig. 7, using the reflection (2) of the diffraction pattern, represents the dark-field image of two different types of crystal. The first type of crystal shown in regions marked A and B in Fig. 6 and region marked C in Fig. 7 is uniform and contains

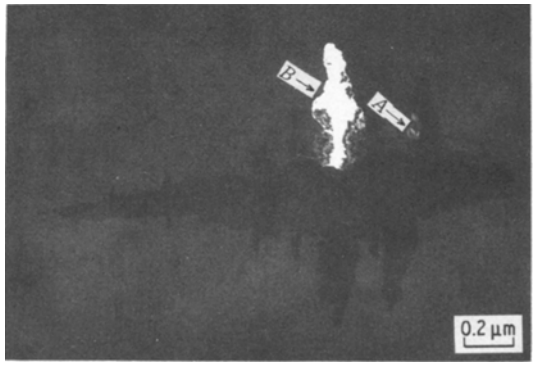


*Figure 6* The corresponding dark-field micrograph of reflection (1) of Fig. 3.


*Figure 7* The corresponding dark-field micrograph of reflection (2) of Fig. 3. The striated crystal in region A represents a twin platelet which corresponds to the matrix spot of reflection (2). The spacing between the lines varies from 3.0 to 6.0 nm.

no striations or fault lines, whereas the second type of crystal shown in the region marked A in Fig. 7 represents a twin platelet which is striated. A comparison between the region marked A in Fig. 6 with that of Fig. 7 reveals that these two types of crystal, that is, the uniform and the striated crystals, overlap. The striations in the striated crystals are irregular and the spacing varies from 3.0 to 6.0 nm in size. This appears to be the first observation of twins with dendritic morphology in amorphous materials.

Fig. 8 represents the corresponding dark-field micrograph using reflection (3) of the diffraction pattern. Again, a comparison between the region marked B in Fig. 6 with that of Fig. 8 and the region marked C in Fig. 7 with that of Fig. 8 indicates the overlapping of two different types of crystal; uniform and twin platelet crystals.

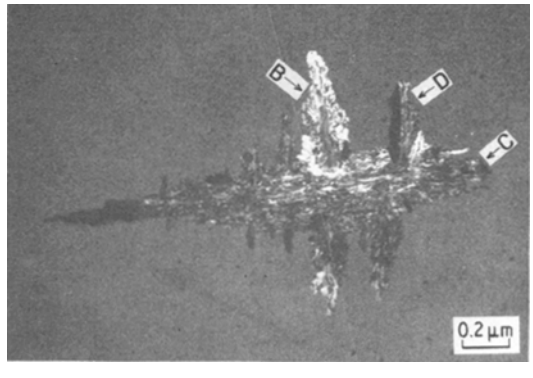


*Figure 8* The corresponding dark-field micrograph of reflection (3) of Fig. 3. A comparison between regions C of this figure and Fig. 7 and regions B of this figure and Fig. 6 reveals that two types of crystal are overlapped: uniform and twin platelet crystals.

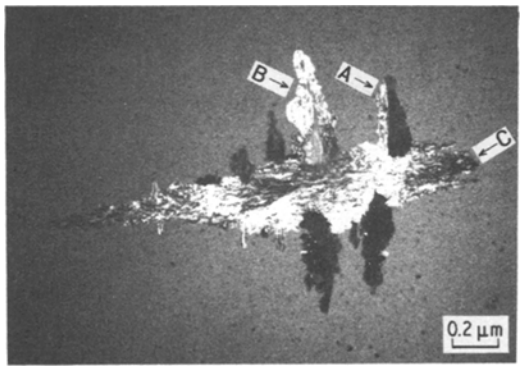


*Figure 9* The corresponding dark-field micrograph of reflection (4) of Fig. 3. A uniform and a striated crystal are overlapped in regions A, B and C.

This can also be seen from Fig. 9 which represents the corresponding dark-field micrograph of reflection (4) of the diffraction pattern. As before, a comparison between regions marked C in Figs 7 and 9 and regions marked B in Figs 6 and 9 indicates that in one branch of the dendrite two different crystal types which are parallel to the plane of the film overlap: uniform and striated types. Figs 6 to 9 also show an interesting branch arm in regions marked A and D.* The arm appears to be composed of a striated bicrystal with a grain boundary running parallel to the centreline of the arm and perpendicular to the film plane.

One possible explanation for the complex diffraction pattern and interesting sequence of dark-field image formations is that the dendrite is composed of several overlapping crystals. When a beam of electrons is incident on a single crystal, the reflected rays form a diffraction pattern; a particular $(h\,k\,l)$ plane forms a single reflection point on that pattern. If a dark-field image is formed with a particular $(h\,k\,l)$ reflection, the entire crystal is viewed provided there is no bending of the crystal (e.g. bend contour). Imaging with another $(h\,k\,l)$ reflection will also show the same crystal. With this in mind, contrast the behaviour observed in the dark-field sequence, Figs 6 to 9, which show that the dendrite is composed of many overlapping crystals; when imaged with reflection (3) on the diffraction pattern, nearly all of the dendrite is seen, yet when reflections (1) and (2) are used to make the image, only crystals in regions A, B and C are seen. It is doubtful that bending of the dendrites (e.g. bend contours) is the cause of the observed behaviour because the "roots" of individual side-arm crystals appear to divide the regions of sharp contrast and these "roots" appear to occur exactly at the same position in each figure. This feature of the dendrites could be explained by assuming that, in regions marked B and C, crystals parallel to the plane of the film overlap other crystals with different orientations.

## 4. Conclusions

(1) In contrast to the behaviour observed in the case of the $Ni_xP_x$(Ni) morphologies, the dendritic morphologies are crystal structure dependent.

(2) The morphologies of the dendrite depend on the rates of electron-beam heating, temperature gradients and homogeneity of the as-deposited films.

(3) The presence of uniform crystals at the interface of the dendrites and/or amorphous region is due to local variation of composition in the as-deposited films.

(4) The presence of micro-crystalline regions in the as-deposited films is due to local variation of composition in the as-deposited films.

(5) The tendency for dendritic formation is the highest in regions which have the highest thermal conductivity (i.e. regions of high Ni to P concentration ratio).

(6) The dendritic arms are composed of overlapping uniform crystals and striated bicrystals; the grain boundary of striated bicrystal runs parallel to the centreline of the arm and perpendicular to the surface of the film.

## References

1. P. D. DUWEZ and J. DIXMIER, *J. Appl. Phys.* **44** (1973) 1189.
2. A. K. SINHA, B. C. GUIESSEN and D. E. POLK, "Treatise on Solid State Chemistry", Vol. 3, Crystalline and Noncrystalline Solids, edited by N. B. Hannay (Plenum Press, New York, 1971) pp. 1–80.
3. T. MASUMOTO and R. MADDIN, *Mater. Sci. Eng.* **19** (1975) 19.
4. *Idem, ibid.* **23** (1976) 23.
5. T. WATANABE and Y. TANABE, *ibid.* **23** (1976) 97.
6. P. DUHAJ, V. SLADEK and P. MARFKO, *J. Non-Cryst. Solids* **13** (1973) 341.
7. P. DUHAJ, D. BARANCOK and A. ONDREJKA, *ibid.* **21** (1976) 411.
8. T. MASUMOTO and R. MADDIN, *Acta Met.* **19** (1971) 725.

*The region marked D is imaged using reflection (3) of Fig. 3.

9. E. VAFAEI-MAKHSOOS, EDWIN L. THOMAS and LOUIS E. TOTH, *Met. Trans.* **9A** (1978) 1449.
10. E. VAFAEI-MAKHSOOS, *J. Appl. Phys.* **51** (1980) 6366.
11. R. H. WILLENS, *ibid.* **33** (1962) 3269.
12. B. G. BAGLEY and D. TURNBULL, *Acta Met.* **18** (1970) 857.

Received 15 September 1980 and accepted 12 January 1981.